# Decadal observations of deep ocean temperature change passively probed with acoustic waves

Läslo G. Evers

Check for updates

View Online

Export Citation

---

**Articles You May Be Interested In**

Ocean soundscapes and trends from 2003 to 2021: 10–100 Hz

*J. Acoust. Soc. Am.* (June 2025)

Variability of the coherent arrivals extracted from low-frequency deep-ocean ambient noise correlations

*J. Acoust. Soc. Am.* (August 2015)

Passive probing of the sound fixing and ranging channel with hydro-acoustic observations from ridge earthquakes

*J. Acoust. Soc. Am.* (April 2015)

# Decadal observations of deep ocean temperature change passively probed with acoustic waves

Läslo G. Evers[1,2]

[1]Research and Development Department of Seismology and Acoustics, Royal Netherlands Meteorological Institute (KNMI), De Bilt, the Netherlands
[2]Department of Geoscience and Engineering, Faculty of Civil Engineering and Geosciences, Delft University of Technology, Delft, the Netherlands

evers@knmi.nl

**Abstract:** The oceans are filled with acoustic waves, which are trapped in a low-velocity layer at about 1 km water depth. The sound speed depends on the temperature. From hydroacoustic arrays, travel times can be obtained through cross-correlating transient signals. Hydroacoustic station H10 (Ascension Island) appeared capable of measuring deep ocean temperature change. A decrease in modeled and observed travel times of $-0.002$ s/yr was derived between two arrays, corresponding to a warming of $0.007\,°C$/yr, at about 900 m water depth over two decades. As such, acoustic waves provide an independent and passively acquired measure of the temperature change in the deep ocean. © 2025 Author(s). All article content, except where otherwise noted, is licensed under a Creative Commons Attribution (CC BY) license (https://creativecommons.org/licenses/by/4.0/).

## 1. Introduction

The Comprehensive Nuclear-Test-Ban Treaty (CTBT) is verified with the International Monitoring System (IMS). The IMS consists of seismological and infrasonic stations to monitor, respectively, the solid earth and atmosphere for nuclear-test explosions. These so-called waveform technologies provide an indirect measure of a possible nuclear test explosion. In addition, radio-nuclides and noble gasses are measured in the atmosphere as actual indicators of a nuclear test (Dahlman et al., 2009).

In this study, hydroacoustical measurements of the IMS are used, which are in place to monitor the oceans for explosions. Two types of measurements of this waveform technology are being applied in the IMS: (1) *T*-phase stations on steep-sloped oceanic islands and (2) hydrophone stations in the deep oceans. The *T*-phase stations are seismometers which measure seismic waves that result from the conversion of hydroacoustic waves (Stevens et al., 2021). Hydrophone stations consist of three-element arrays, i.e., triplets, located in the sound fixing and ranging (SOFAR) channel (De Groot-Hedlin and Orcutt, 2001; Gibbons, 2022). The SOFAR channel is a low-velocity layer which traps hydroacoustical waves at approximately 1 km water depth. The low-frequency contents of the waves and ducting properties of the channel ensure detections over long ranges as the attenuation is limited (Munk and Forbes, 1989).

The sound speed in the ocean depends on pressure, salinity, and temperature. Fluctuations in the sound speed are primarily driven by ocean temperatures (Munk et al., 1995). Therefore, changes in the travel time of acoustic waves can be attributed to temperature changes. Acoustic travel times can be passively estimated using diffuse ambient sound with cross-correlation calculations. Furthermore, transient signals and/or active sources can be used to probe the oceans temperature. The use of acoustic travel times from ambient noise for estimating the deep ocean temperature has recently been applied by Ragland et al. (2024), and references therein give an overview of past studies performed. Dushaw et al. (2009) show how an active source can be used to estimate basin-scale deep ocean temperature, following earlier studies on ocean acoustic tomography and thermometry (Munk and Wunsch, 1979; Cornuelle et al., 1993; Dushaw, 2003). Wu et al. (2020) and Wu et al. (2023) used transient signals from earthquakes, so-called *T*-waves, for estimating temperature through seismic ocean thermometry (SOT). Peng et al. (2024) successfully applied SOT to repeating earthquakes in obtaining deep ocean temperature variability.

IMS hydroacoustic station H10 is located in the Atlantic Ocean near Ascension Island (see Fig. 1). Two hydrophone arrays are situated to the north (H10N) and south (H10S) of the island at an inter-array distance of 125 km. The arrays have an aperture of about 2 km and are placed in the SOFAR channel at a depth of 875 m (Metz et al., 2016). Data from H10 is available from early 2005 to now. This study uses data from H10; previous studies using H10 data include acoustic thermometry of the deep oceans with ambient noise (Woolfe et al., 2015; Woolfe and Sabra, 2015), probing the SOFAR channel with earthquake signals (Evers and Snellen, 2015), modeling long-range sound propagation in the SOFAR channel (Heaney and Campbell, 2016), the use of ambient noise in retrieving the crustal structure (Ball et al., 2016), cross-correlations of single hydrophone pairs and array beams of ambient noise to retrieve the deep ocean sound
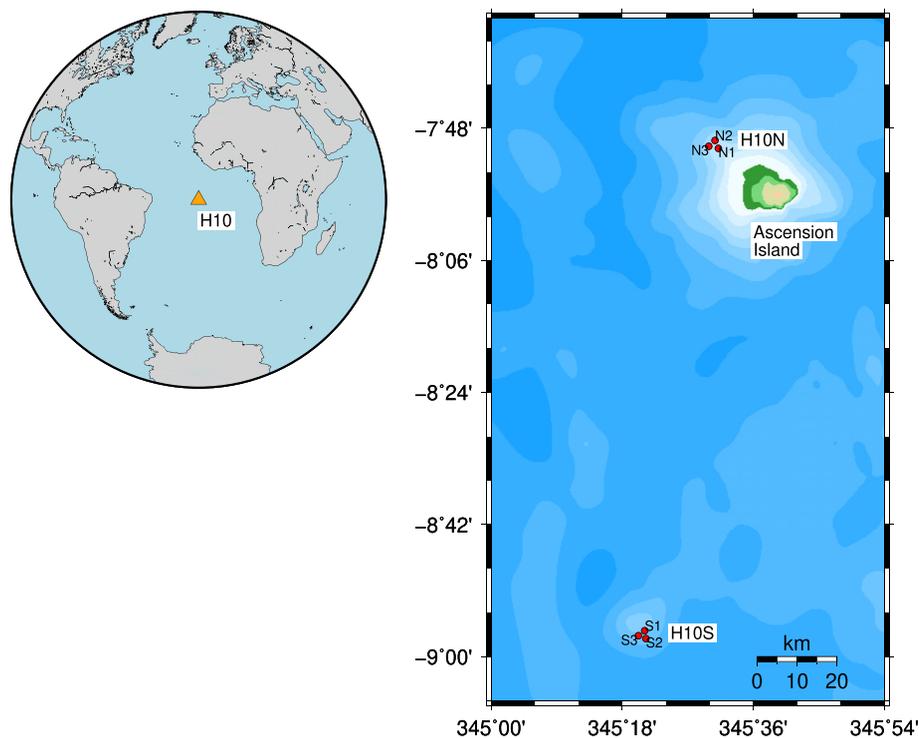
Fig. 1. Hydroacoustic station H10 is located in the Atlantic Ocean near Ascension Island. H10 consists of two hydrophone arrays, i.e., a northern (H10N) and southern array (H10S). Each array is configured with three hydrophones, a so-called triplet, with an aperture of about 2 km at 875 m water depth. Continuous data are available from 3/23/2005 and onward (data for hydrophone S1 are included until October 2013).

speed (Evers *et al.,* 2017), and studying submarine volcanic eruptions (Metz *et al.,* 2016; Smets *et al.,* 2022). Furthermore, H10 data were extensively used for localizing the Argentine submarine ARA San Juan that went missing in November 2017 (Dall'Osto, 2019; Heyburn *et al.,* 2020; Nielsen *et al.,* 2021; Vergoz *et al.,* 2021).

This letter is organized as follows. Section 2 describes how the automatic detections at H10 from coherent arrivals from transient signals are used to estimate acoustic travel times between the hydrophone arrays. A trend found in the travel times is assessed in Sec. 3. Section 4 further refines this travel time analysis by cross-correlating the actual waveforms between hydrophone pairs of the arrays. The resulting trends in travel times are used to infer ocean temperatures which agree with ocean model predictions of temperature, as discussed in Sec. 5. It is concluded in Sec. 6 that H10 acts as a continuous thermometer in the deep ocean capable of sensing decadal temperature variability.

## 2. Detections

In this section, nearly two decades of detections at H10 are evaluated in terms of acoustic travel times.

The continuous data from H10 is automatically processed at the International Data Centre (IDC) of the Comprehensive Nuclear-Test-Ban Treaty Organization (CTBTO). A detector is applied to the individual hydrophone recordings. This detector is based on short-term average/long-term average (STA/LTA) calculations. The individual detections are combined into an array detection through a closure relation, which is the sum of the average travel times between the hydrophones with respect to the center of the array. This relation ideally sums up to zero; in practice, a small threshold is set to allow for signals with a low signal-to-noise ratio to be detected. From the array detection, a slowness and back azimuth are derived.

The automatic detections provided by the IDC are evaluated with the aim to obtain the travel time between H10N and H10S. First, detections are selected with a similar slowness per array. Second, if the travel time between H10N and H10S is within −120 and 120 s, the detections at both arrays are assumed to be associated. This means that the same coherent acoustic wave was detected at H10N and H10S. Most likely, this association relates to a common source for the detections.

A minus sign means the coherent wave traveled from H10N to H10S and, thus, comes from a northerly direction (and vice versa for the plus sign). Travel times of 0 s indicate that the source is located halfway between H10N and H10S on a roughly east-west trending line. Data of hydrophone S1 (H10S) is available until October 2013. To create a homogeneous set of travel times, only hydrophone S2 and S3 are used in the above analysis for the entire period. A total of 81 043 travel times between H10N and H10S are retrieved for the period 3/23/2005 through 10/28/2024 and depicted in Fig. 2.
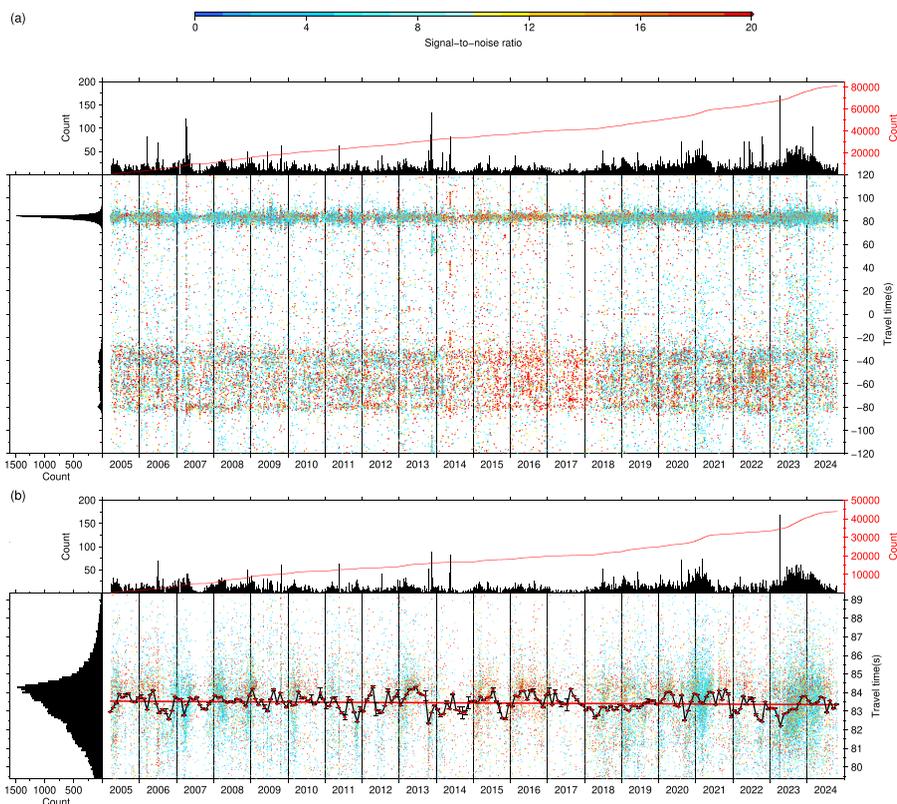
Fig. 2. The travel time between H10N and H10S as a function of time, where the average signal-to-noise ratio of the array detections are color coded. (a) The travel time in the range of −120 to 120 s. A minus sign means the detection first occurred at H10N and then at H10S. This implies a common source to the north of H10 (and vice versa for the plus sign). The histogram on top shows the number of detections per day (black) and the cumulative number of detections (red), i.e., 81 043 in total. The histogram to the left shows the sum of the travel times. (b) The representation is the same as that in (a) with a zoom-in of the peak of 84.4 s. The average travel times per month (red dots, with standard deviations) and the trend (red) through these averages are also displayed. The trend is found to be −0.01 ± 0.005 s/yr in these 43 908 detections.

From Fig. 2(a), it follows that coherent waves travel from H10S to H10N, adding up to a peak in the travel time distribution of 84.4 s. Coherent waves coming from northerly directions are more scattered and show up with travel times between −25 and −85 s. Figure 2(b) zooms into the peak of 84.4 s; 43 908 detections are shown. A yearly repetitive pattern is visible in the detection rate. Most detections appear to take place at the beginning of the year, although large variations from year to year are present. Average travel times per month are calculated and shown in Fig. 2(b). A trend of −0.01 ± 0.005 s/yr is found in these travel times, which translate to a reduction of 0.19 s (from 83.54 to 83.35 s) over the period analyzed. This trend is significant as the error is an order of magnitude smaller than the value itself. The trend and its standard error are calculated with the method of least squares (Squires, 2001).

In Secs. 3–5, it will be investigated whether the change in travel time can be attributed to a change in sound speed and, hence, for example, a temperature change.

## 3. Deep ocean temperature, sound speed, and travel time

This section describes the influence of temperature variability on deep ocean acoustic travel times.

Munk and Forbes (1989) estimated an average warming of 0.005 °C/yr globally at the axis of the SOFAR channel under climate-induced changes. A value for which order of size was confirmed by Messias and Mercier (2022), where a global increase in deep ocean temperature of 0.2 °C was estimated for the next 50 years (i.e., 0.004 °C/yr). Bagnell and DeVries (2021) found a substantial acceleration in warming rates after 1990 in the entire water column in most of the world's oceans, including the area and depth in this study, with the deep ocean switching from cooling to warming.

For the location of H10, the Global Ocean Physics Reanalysis GLORYS12V1 product of Copernicus provides the temperature at around 900 m water depth. GLORYS12V1 assimilates observations such as those from Argo floats (Wong et al., 2020). These are especially relevant for the target depth in this study, where actual measurements of temperature are rare.

In Fig. 3(a) the values since 1/1/1993 are shown, and a significant trend of 0.0061 °C/yr is found. The trend for the period of interest, i.e., since 3/2005, is larger with 0.0086 °C/yr.
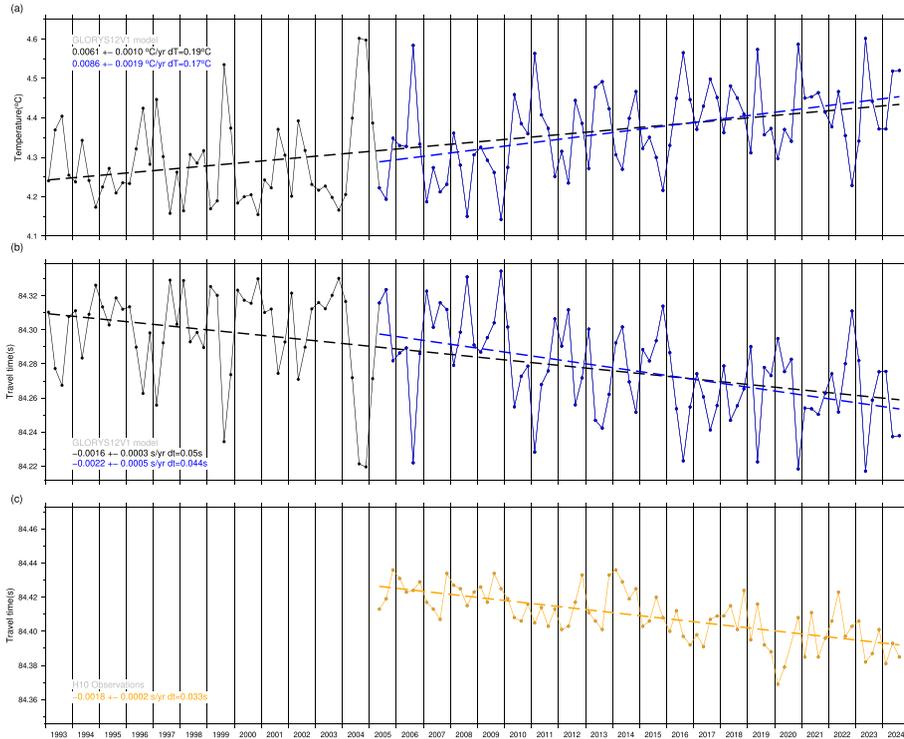
Fig. 3. The temperature and modeled and observed travel times. (a) The temperatures from GLORYS12V1 specifications at the location 14.5 W, 8.5 S at 902.34 m water depth are displayed. Quarterly average values and their trends are shown for the whole period provided by the model (since 1991 in black) and the period of interest (since March 2005 appears in blue). (b) The derived travel times between H10N and H10S over 125 km, from GLORYS12V1 specifications are depicted. The temperature increase found in (a) leads to an increase in the sound speed and, hence, a reduction in travel time over the period of interest with a significant trend. (c) The reduction in travel time from H10 observations is shown.

The sound speed is parameterized as

$$c(z) = 1449.2 + 4.6T(z) - 0.055T^2(z) + 0.00029T^3(z) + (1.34 - 0.01T(z))(S(z) - 35) + 0.016z, \quad (1)$$

where $c(z)$ is the sound speed in m/s as a function of depth $z$, $T(z)$ is the depth-dependent temperature in centigrade, and $S(z)$ is the depth-dependent salinity in parts per thousand (Jensen *et al.*, 2000). From the GLORYS12V1 specifications, the temperature is expected to increase from 4.29 to 4.45 °C. This translates to an increase in sound speed of 0.8 m/s and reduction in the travel time of 0.044 s between H10N and H10S over a distance of 125 km [see Fig. 3(b)].

The salinity increases from 34.50 to 34.52 ppt over the period of interest. This leads to a small change in the sound speed of 0.026 m/s. Although taken into account, this change is too small to affect the travel time.

In travel time analysis, a reduction of 0.19 s was found (see Sec. 2). The apparent reduction in the observed travel time appears too large to be solely explained by deep ocean warming.

In Sec. 4, the analysis of H10 recordings will be refined by processing the actual waveforms of the events rather than the derived detections in an attempt to sharpen the travel time distribution.

### 4. Trends in travel time from cross-correlating event waveforms

In this section, the waveforms of the 43 908 events obtained in Sec. 2 are further analyzed to more accurately derive the travel times between H10N and H10S. For each event, a waveform segment of 120 s around the detection time is acquired for the different hydrophones, i.e., N1, N2, and N3 and S2 and S3. Next, the cross-correlation between each hydrophone pair is calculated from H10N and H10S. Prior to this, the waveforms are bandpass filtered with a second order Butterworth filter with corner frequencies of 3 and 20 Hz.

Figure 4 shows the results for each hydrophone pair. In the top frames, the cross-correlation functions (CCFs) per event are given. The grand average over all events is displayed to the left with its envelop (in red). The bottom frames zoom into the CCFs, which are quarterly averaged to stabilize the results. The maxima (or minima) are picked on the basis of the highest value of the grand average, which is determined with the envelop. Trends are calculated (orange lines) on the basis of these quarterly travel time values (orange crosses). A consistent trend between all hydrophone pairs is found and ranges from −0.0016 to −0.0020 s/yr, i.e., a statistically significant decrease in travel time over nearly two decades of

recordings. (The third quarter of 2020 has been removed from the trend analysis as multiple maxima of the CCFs are present over a broad travel time range.) The trend from cross-correlations is an order of magnitude smaller than the trend from the detections (in Sec. 2).

A sanity check is performed by also calculating the CCFs and their trends between the hydrophones of an array. The results show, as expected, no trends because of the small distances between the array elements. It also reveals that, for example, instrumental drift or other acquisition related issues are not present and could erroneously be interpreted as a change in the medium.

In Sec. 5, the cross-correlation results will be discussed in physical terms and compared to modeled travel times and temperature variability.

## 5. Discussion

A distinct peak in travel time is found in the analysis of the detections (Sec. 2) and cross-correlation calculations (Sec. 4), and its physical meaning and relation to temperature variability will be discussed here.

The peak resembles the stationary phase, which has been found by interferometric approaches to ambient noise (Evers et al., 2017; Ragland et al., 2024). In such studies, the ambient noise field is homogeneously distributed around the hydrophones, which allows for the interchange of sources and receivers through reciprocity. Here, transient signals are used rather than ambient noise. However, as the travel time between H10N and H10S is resolved, similarities between both techniques are obvious. In this study, only positive travel times are stationary resolved, which implies that the sources of the transient signals are located to the south of H10. Combined with the fact that periods of high detection rates occur in austral summer [see, e.g., 2007, 2008, and 2021 in Fig. 2(b)], sources are most likely associated with ice-related activity on and near Antarctica, which is in the acoustic line of sight (Woolfe and Sabra, 2015). Sources of acoustic waves are glacier dynamics, such as calving of icebergs, and the interaction of icebergs in open water and with the ocean floor (Evers et al., 2013; Sambell et al., 2019; Schlindwein, 2024). Each of these events has a specific location. This can be observed in Fig. 2(b), where the average of the histogram lies at 83.4 s and its peak is at 84.4 s. Time averaging the CFFs aids in stabilizing the results by compensating for this non-diffusivity and propagation effects in the wavefield (Godin, 2012; Skarsoulis and Cornuelle, 2020). I doing so, specific sources in the Fresnel zone of the southern endfire on the azimuth from H10N and H10S are allowed to add to the stationary phase. This is confirmed by the average travel times of all time-averaged CCFs also being 84.4 s (see Fig. 4).

The trends in the travel time differ between the observations (−0.0018 s/yr) and the model (−0.0022 s/yr). Figure 3(c) shows this trend in the observations, which is the average of all trends found in Fig. 4. There are many explanations for this difference in terms of resolution and uncertainties in the observations and model. Most importantly, it should be noted that the values are in close agreement. However, there is a clear discrepancy between the depth of H10, i.e., 875 m, and the model depth of 902.34 m. It appears that the trend is −0.0012 s/yr at 1062.44 m (the next model level). By linear interpolation, the observations and model match −0.0018 s/yr at 974 m, which translates to a temperature increase of 0.0067 °C/yr. The lower temperature at larger depths will also better fit the absolute values of the modeled travel times with respect the observed travel times. However, it should be noted that modal propagation in the sound channel fills the channel with sound, leading to a group velocity, resulting from the depth-integrated temperature. Tomographic and interferometric approaches have also discussed path integrality, e.g., Cornuelle et al. (1993), Dushaw et al. (2009), and Woolfe et al. (2015).

As discussed, there are many other ways to fit the observations to the model and even differences may inherently be present. However, an estimate is provided for the relation between a decrease in travel time (−0.002 s/yr) versus an increase in temperature (0.007 °C/yr).

Woolfe et al. (2015) found a trend of 0.013 °C/yr for H10 with weekly averages of cross-correlations of ambient noise for the period of 2006–2013. A similar trend is present in the GLORYS12V1 specifications for that period, i.e., 0.014 °C/yr corresponding to −0.0038 s/yr. The quarterly averages presented here for that period only show a slightly higher value of −0.0019 s/yr than the overall trend (−0.0018 s/yr). Monthly averaging shows a stronger trend (e.g., −0.0025 ± 0.0015 s/yr for N1-S2). However, the errors become too large to retrieve significant trends as transient events are less abundantly present compared to the more continuous ambient noise.

## 6. Conclusion

Hydroacoustic station H10, located near Ascension Island in the Atlantic Ocean, has been providing data for nearly two decades. Although in place to detect nuclear-test explosion, H10 with its two arrays at 125 km distance can also be used to measure the deep ocean temperature. Events detected on both arrays have been cross-correlated to obtain an accurate measure of the travel time. This travel time appeared to reduce at a rate of 0.0018 s/yr. Deep ocean warming leads to an increase in the sound speed and, hence, a decrease in the travel time. This warming was found to be 0.0067 °C/yr from model specifications at around 900 m water depth. Taking the uncertainties in the observations and model into account, an estimate is provided of −0.002 s/yr travel time reduction as a result of 0.007 °C/yr temperature increase over nearly two decades.
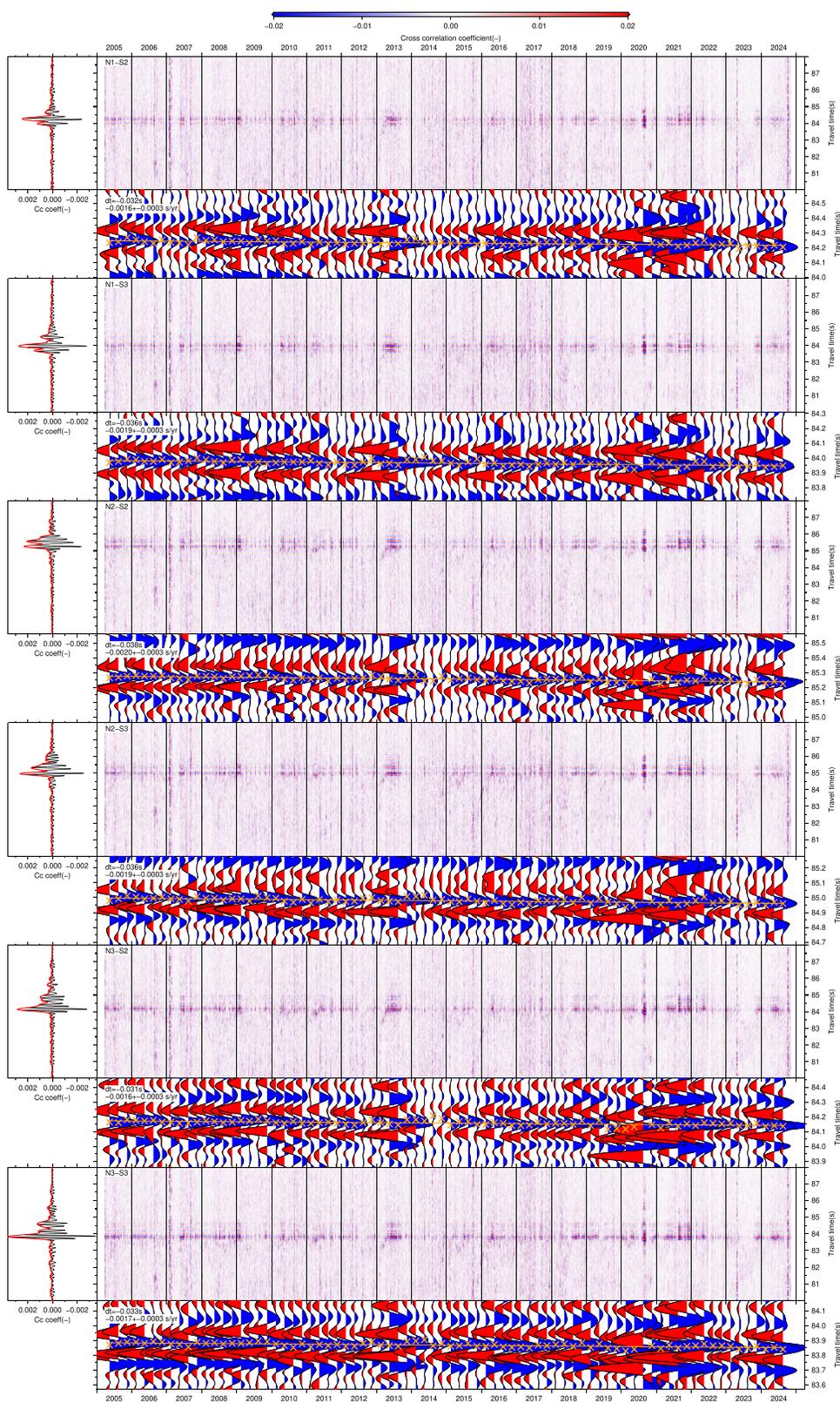
Fig. 4. Cross-correlation functions (CCFs) of the hydrophone pairs of H10N and H10S. From top to bottom, N1-S2, N1-S3, N2-S2, N2-S3, N3-S2, and N3-S3 are shown. For each pair, the CCFs per event are given (top frames), including a zoom-in into the quarterly averaged CCFs (lower frames). The maxima (or minima) are selected (orange crosses) on the basis of the grand-average envelope (red line), which are shown in the frames to the left. Trends and total reductions in travel times are given in quarterly averaged frames.

Such warming is also relevant for marine life. Affatati *et al.* (2022) assessed the (deep) ocean sound speed changes under future warming and its relation to marine mammals as it may affect communication, feeding, predator avoidance, and navigation (Venegas *et al.*, 2023).

It is concluded that hydroacoustic stations can provide an independent measure of the changing temperatures in the deep ocean. Such observations can be passively obtained and even as a by-product from existing monitoring networks. Future studies will concentrate on applying the techniques presented here to these networks and other IMS stations.

### Author Declarations
*Conflict of Interest*

The authors have no conflicts to disclose.

### Data Availability

The data that support the findings of this study are openly available in the CTBTO's virtual Data Exploitation Centre (vDEC https://www.ctbto.org/specials/vdec/) at https://www.ctbto.org/resources/for-researchers-experts/vdec/request-for-data (Gibbons, 2022).

### References

[1]See https://doi.org/10.48670/moi-00021 (Last viewed July 10, 2025).
[2]See https://ds.iris.edu/ds/nodes/dmc/forms/sac/ (Last viewed July 10, 2025).

Affatati, A., Scaini, C., and Salon, S. (**2022**). "Ocean sound propagation in a changing climate: Global sound speed changes and identification of acoustic hotspots," Earth's Future **10**(3), e2021EF002099.

Bagnell, A., and DeVries, T. (**2021**). "20th century cooling of the deep ocean contributed to delayed acceleration of Earth's energy imbalance," Nat. Commun. **12**, 4604.

Ball, J. S., Godin, O. A., Evers, L. G., and Lv, C. (**2016**). "Long-range correlations of microseism-band pressure fluctuations in the ocean," Geophys. J. Int. **206**(2), 825–834.

Cornuelle, B. D., Worcester, P. F., Hildebrand, J. A., Hodgkiss, W. S., Jr., Duda, T. F., Boyd, J., Howe, B. M., Mercer, J. A., and Spindel, R. C. (**1993**). "Ocean acoustic tomography at 1000-km range using wavefronts measured with a large-aperture vertical array," J. Geophys. Res. Oceans **98**(C9), 16365–16377, https://doi.org/10.1029/93JC01246

Dahlman, O., Mykkeltveit, P., and Haak, H. (**2009**). "Monitoring technologies," in *Nuclear Test Ban* (Springer, Dordrecht), Chap. 2, pp. 1–34.

Dall'Osto, D. R. (**2019**). "Source triangulation utilizing three-dimensional arrivals: Application to the search for the ARA San Juan submarine," J. Acoust. Soc. Am. **146**(3), 2104–2112.

De Groot-Hedlin, C., and Orcutt, J. (**2001**). "Monitoring the comprehensive nuclear-test-ban treaty," Pure Appl. Geophys. **158**, 421–626.

Dushaw, B. (**2003**). "Acoustic thermometry in the North Pacific," Clivar Exch. **8**, 1–5.

Dushaw, B. D., Worcester, P. F., Munk, W. H., Spindel, R. C., Mercer, J. A., Howe, B. M., Metzger, K., Birdsall, T. G., Andrew, R. K., Dzieciuch, M. A., Cornuelle, B. D., and Menemenlis, D. (**2009**). "A decade of acoustic thermometry in the North Pacific Ocean," J. Geophys. Res. **114**(C7), C07021, https://doi.org/10.1029/2008jc005124

Evers, L. G., Green, D. N., Young, N. W., and Snellen, M. (**2013**). "Remote hydroacoustic sensing of large icebergs in the southern Indian Ocean: Implications for iceberg monitoring," Geophys. Res. Lett. **40**(17), 4694–4699, https://doi.org/10.1002/grl.50914

Evers, L. G., and Snellen, M. (**2015**). "Passive probing of the sound fixing and ranging channel with hydro-acoustic observations from ridge earthquakes," J. Acoust. Soc. Am. **137**(4), 2124–2136.

Evers, L. G., Wapenaar, K., Heaney, K. D., and Snellen, M. (**2017**). "Deep ocean sound speed characteristics passively derived from the ambient acoustic noise field," Geophys. J. Int. **210**(1), 27–33.

Gibbons, S. J. (**2022**). "The hydroacoustic network of the CTBT International Monitoring System: Access and exploitation," J. Peace Nucl. Disarmament **5**(2), 452–468.

Godin, O. (**2012**). "On the possibility of using acoustic reverberation for remote sensing of ocean dynamics," Acoust. Phys. **58**, 129–138.

Heaney, K. D., and Campbell, R. L. (**2016**). "Three-dimensional parabolic equation modeling of mesoscale eddy deflection," J. Acoust. Soc. Am. **139**(2), 918–926.

Heyburn, R., Bowers, D., and Green, D. N. (**2020**). "Seismic and hydroacoustic observations from recent underwater events in the South Atlantic Ocean," Geophys. J. Int. **223**(1), 289–300.

Jensen, F., Kuperman, W., Porter, M., and Schmidt, H. (**2000**). *Computational Ocean Acoustics* (Springer, New York).

Messias, M.-J., and Mercier, H. (**2022**). "The redistribution of anthropogenic excess heat is a key driver of warming in the North Atlantic," Commun. Earth Environ. **3**, 118.

Metz, D., Watts, A. B., Grevemeyer, I., Rodgers, M., and Paulatto, M. (**2016**). "Ultra-long-range hydroacoustic observations of submarine volcanic activity at Monowai, Kermadec Arc," Geoph. Res. Lett. **43**(4), 1529–1536.

Munk, W., Worcester, P., and Wunsch, C. (**1995**). *Ocean Acoustic Tomography* (Cambridge University Press, Cambridge, UK), pp. 1–29.

Munk, W., and Wunsch, C. (**1979**). "Ocean acoustic tomography: A scheme for large scale monitoring," Deep Sea Res. **26**, 123–161.

Munk, W. H., and Forbes, A. M. G. (**1989**). "Global ocean warming: An acoustic measure?," J. Phys. Oceanogr. **19**(11), 1765–1778.

Nielsen, P. L., Zampolli, M., Bras, R. L., Mialle, P., Bittner, P., Poplavskiy, A., Rozhkov, M., Haralabus, G., Tomuta, E., Bell, R., Grenard, P., Taylor, T., and Özel, N. M. (**2021**). "CTBTO's data and analysis pertaining to the search for the missing Argentine submarine ARA San Juan," Pure Appl. Geophys. **178**, 2557–2577.

Peng, S., Callies, J., Wu, W., and Zhan, Z. (**2024**). "Seismic ocean thermometry of the Kuroshio extension region," J. Geophys. Res. **129**(2), e2023JC020636, https://doi.org/10.1029/2023JC020636.

Ragland, J., Abadi, S., and Sabra, K. (**2024**). "Using ocean ambient sound to measure local integrated deep ocean temperature," Geophys. Res. Lett. **51**(12), e2024GL108943, https://doi.org/10.1029/2024GL108943

Sambell, K. A. M., Smets, P. S. M., Simons, D. G., Snellen, M., and Evers, L. G. (**2019**). "A study on the ambient noise field at a hydroacoustic array near Robinson Crusoe Island," Geophys. J. Int. **218**(1), 88–99.

Schlindwein, V. (**2024**). *Iceberg Noise* (American Geophysical Union (AGU), Washington, DC), Chap. 6, pp. 83–96.

Skarsoulis, E. K., and Cornuelle, B. D. (**2020**). "Cross-correlation sensitivity kernels with respect to noise source distribution," J. Acoust. Soc. Am. **147**(1), 1–9.

Smets, P. S. M., Weemstra, C., and Evers, L. G. (**2022**). "Hydroacoustic travel time variations as a proxy for passive deep-ocean thermometry—A cookbook," J. Geophys. Res.: Oceans **127**(5), e2022JC018451, https://doi.org/10.1029/2022JC018451.

Squires, G. L. (**2001**). *Further Topics in Statistical Theory* (Cambridge University Press, Cambridge, UK), pp. 30–32.

Stevens, J., Hanson, J., Nielsen, P., Zampolli, M., Bras, R. L., Haralabus, G., and Stevens, M. (**2021**). "Calculation of hydroacoustic propagation and conversion to seismic phases at *T*-stations," Pure Appl. Geophys. **178**, 2579–2609.

Venegas, R. M., Acevedo, J., and Treml, E. A. (**2023**). "Three decades of ocean warming impacts on marine ecosystems: A review and perspective," Deep Sea Res. Part II **212**, 105318.

Vergoz, J., Cansi, Y., Cano, Y., and Gaillard, P. (**2021**). "Analysis of hydroacoustic signals associated to the loss of the Argentinian ARA San Juan submarine," Pure Appl. Geophys. **178**, 2527–2556.

Wessel, P., Smith, W. H. F., Scharroo, R., Luis, J., and Wobbe, F. (**2013**). "Generic mapping tools: Improved version released," EoS. Trans., Am. Geophys. Union **94**(45), 409–410.

Wong, A. P. S., Wijffels, S. E., Riser, S. C., Pouliquen, S., Hosoda, S., Roemmich, D., Gilson, J., Johnson, G. C., Martini, K., Murphy, D. J., Scanderbeg, M., Bhaskar, T. V. S. U., Buck, J. J. H., Merceur, F., Carval, T., Maze, G., Cabanes, C., André, X., Poffa, N., Yashayaev, I., Barker, P. M., Guinehut, S., Belbéoch, M., Ignaszewski, M., Baringer, M. O., Schmid, C., Lyman, J. M., McTaggart, K. E., Purkey, S. G., Zilberman, N., Alkire, M. B., Swift, D., Owens, W. B., Jayne, S. R., Hersh, C., Robbins, P., West-Mack, D., Bahr, F., Yoshida, S., Sutton, P. J. H., Cancouët, R., Coatanoan, C., Dobbler, D., Juan, A. G., Gourrion, J., Kolodziejczyk, N., Bernard, V., Bourlès, B., Claustre, H., D'Ortenzio, F., Le Reste, S., Le Traon, P.-Y., Rannou, J.-P., Saout-Grit, C., Speich, S., Thierry, V., Verbrugge, N., Angel-Benavides, I. M., Klein, B., Notarstefano, G., Poulain, P.-M., Vélez-Belchí, P., Suga, T., Ando, K., Iwasaska, N., Kobayashi, T., Masuda, S., Oka, E., Sato, K., Nakamura, T., Sato, K., Takatsuki, Y., Yoshida, T., Cowley, R., Lovell, J. L., Oke, P. R., van Wijk, E. M., Carse, F., Donnelly, M., Gould, W. J., Gowers, K., King, B. A., Loch, S. G., Mowat, M., Turton, J., Rama Rao, E. P., Ravichandran, M., Freeland, H. J., Gaboury, I., Gilbert, D., Greenan, B. J. W., Ouellet, M., Ross, T., Tran, A., Dong, M., Liu, Z., Xu, J., Kang, K., Jo, H., Kim, S.-D., and Park, H.-M. (**2020**). "Argo Data 1999–2019: Two million temperature-salinity profiles and subsurface velocity observations from a global array of profiling floats," Front. Mar. Sci. **7**, 700.

Woolfe, K. F., Lani, S., Sabra, K. G., and Kuperman, W. A. (**2015**). "Monitoring deep-ocean temperatures using acoustic ambient noise," Geophys. Res. Lett. **42**(8), 2878–2884, https://doi.org/10.1002/2015GL063438

Woolfe, K. F., and Sabra, K. G. (**2015**). "Variability of the coherent arrivals extracted from low-frequency deep-ocean ambient noise correlations," J. Acoust. Soc. Am. **138**(2), 521–532.

Wu, W., Shen, Z., Peng, S., Zhan, Z., and Callies, J. (**2023**). "Seismic ocean thermometry using CTBTO hydrophones," J. Geophys. Res. **128**(9), e2023JB026687, https://doi.org/10.1029/2023JB026687.

Wu, W., Zhan, Z., Peng, S., Ni, S., and Callies, J. (**2020**). "Seismic ocean thermometry," Science **369**(6510), 1510–1515.